Optics Communications 285 (2012) 238–244

Contents lists available at SciVerse ScienceDirect

Optics Communications

journal homepage: www.elsevier.com/locate/optcom

Modal prediction of atmospheric turbulence wavefront for open-loop liquid-crystal adaptive optics system with recursive least-squares algorithm

Chao Liu [a,b], Lifa Hu [a], Zhaoliang Cao [a], Quanquan Mu [a], Li Xuan [a,*]

[a] State Key Laboratory of Applied Optics, Changchun Institute of Optics, Fine Mechanics and Physics, Chinese Academy of Sciences, Changchun, Jilin 130033, China
[b] Graduate School of the Chinese Academy of Sciences, Beijing 100039, China

ARTICLE INFO

Article history:
Received 21 June 2011
Received in revised form 16 September 2011
Accepted 21 September 2011
Available online 12 October 2011

Keywords:
Atmospheric turbulence prediction
Recursive least-squares
Adaptive optics
Liquid crystal

ABSTRACT

For an open-loop liquid-crystal adaptive optics system, its performance is mainly limited by the time delay. We propose a new modal recursive least-squares (RLS) predictive algorithm to overcome this problem. The RLS algorithm has a simple architecture, low computational complexity and a high converging speed. The impact of the number of the foreword prediction frame N and the number of the predictor order M of the RLS predictor is analyzed in detail. The results show that the best foreword prediction frame N must be equal to the system loop delay frame SLDF. The appropriate predictor order M of the RLS predictor is equal to 2 or 3 when there is no measurement noise and it depends on noise ratio N_R when the measurement error cannot be neglected. We present numerical simulations to show the significant improvements brought by the RLS predictor.

1. Introduction

Liquid-crystal (LC) correctors have been shown to have very high precision in generating a desired wavefront [1–3], and have good repeatability and linearity [4], which is beneficial to open-loop control. Our group has reported to use open-loop LC adaptive optics systems (AOS) to observe space objects and human retinas [5–7]. However, the time lag from detection to compensation may have a major limitation to the performance of such a kind of systems, especially to the systems of turbulence compensation.

A priori, the time delay could be reduced by predictors. Indeed several papers have shown that atmospheric turbulence measured by Shack–Hartmann (SH) sensor is predictable [8,9]. Predictors have already been studied in closed-loop AOS based on deformable mirrors (DM) [10–15]. In the open-loop regimes, Michael Lloyd-Hart and Patrick McGuire et al. have concentrated on the linear zonal prediction of wavefront slope [16,17]. Jorgenson, Aitken and Montera et al. have used artificial neural networks to predict turbulence wavefront slope [18–20]. For the zonal slope prediction, it can take good advantage of the wind-velocity information from the wavefront sensor, but it has a relatively larger computational complexity than modal coefficient prediction. For the artificial neural networks, they need a huge number of training data (hundreds of thousands of training frames) and are plagued when running into local minima in the training error surface [17].

The recursive least-squares (RLS) algorithm is a classical adaptive filter algorithm. It has a simple architecture and converges to the most optimized solution with a global minimum error. When it is used for the training of linear predictors, it has been reported that its speed of convergence is two orders of magnitude faster than that of artificial neural network [17]. Furthermore, its computational complexity is small and it can track the dynamic turbulence on real-time. Michael Lloyd-Hart and Patrick McGuire et al. have shown the feasibility of the RLS algorithm to be used for predicting the open-loop zonal slopes of wavefront [17]. However, they have not applied this technique to an open-loop AOS. Due to the millions of pixels of the LC correctors, usually the modal control is employed to an LC AOS. Therefore, it is straightforward to build a modal predictor that directly predicts the modal coefficient of each control mode. Furthermore, the modal prediction has a relatively low computational cost.

In our research, we apply the RLS algorithm to an open-loop LC AOS, and build a modal RLS predictor to process the Zernike coefficients mode by mode. In Section 2, the open-loop predictive architecture and the RLS predictive algorithm are introduced. In Section 3 we discuss the generation of the data used in the simulation of modal RLS prediction. In Section 4, we discuss the prediction tests and results of the RLS predictor, including the choices of the order of the predictor, the number of the forward predictive frames to achieve better results. Finally, in Section 5, we provide the overall conclusions.

* Corresponding author.
E-mail addresses: liuchao678@163.com (C. Liu), xuanli@ciomp.ac.cn (L. Xuan).

0030-4018/$ – see front matter © 2011 Elsevier B.V. All rights reserved.
doi:10.1016/j.optcom.2011.09.061

2. RLS modal predictive algorithm

2.1. Open-loop modal predictive architecture of LC AOS

The block diagram of a typical open-loop modal prediction of an LC AOS is shown in Fig. 1. A predictive correction loop includes several steps. First, the wavefront sensor (WFS) collects light and reads out the data. Second, the control computer begins to calculate the centroids of light spots and local slopes, and then reconstructs the Zernike coefficients. Third, the RLS predictor estimates a new set of Zernike coefficients based on several group of previous reconstructed Zernike coefficients. Finally, according to the estimated Zernike coefficients, a gray map (quantified wavefront map to drive the LC corrector) is calculated and sent to the head of a liquid-crystal on silicon (LCOS) wavefront corrector. After the transmission of the gray map and the response of LC steps are finished, the turbulence wavefront is corrected. The gray map is holding on the LCOS until the next new gray map is transmitted to the LCOS.

The time series of a predictive correction loop includes exposure time (1 ms), data outputting time (1 ms), calculating time (0.6 ms), data transmission time (0.4 ms), and LC response time (2 ms). These times match the time consumption of a new LC AOS designed by ourselves recently. The calculating time includes the times of centroid and slope calculation, Zernike coefficient reconstruction, RLS prediction and gray map calculation. The total delay time of a correction loop is 5.0 ms [see Fig. 2]. As the sampling frequency is 1000 Hz (a frame transfer mode is used), the system loop delay frame (SLDF) is 5. This is a very important factor that needs to be considered for the RLS predictor to improve the system performance.

It is should be noted that the sampling frequency f_s of the WFS is 1000 Hz, but the correction frequency of the LCOS is only 500 Hz [1/(2 ms)]. It attributes to the mismatch of the exposure time and the LC response time. In this case, the gray map is calculated for every frame, but only the odd frames are sent to the LCOS. It is obvious that the reconstructed frequency of the Zernike coefficients for the RLS predictor is equal to the sampling frequency f_s of the WFS, which equals to 1000 Hz for the actual LC AOS.

2.2. The RLS algorithm for modal turbulence prediction

RLS predictor is an expansion of the RLS filter which is an adaptive, time-update version of filter. The purpose of the RLS predictor is to minimize the weighted sum of squared predictive error. When given a time array of a certain Zernike coefficient [$c(1)$, $c(2)$, ..., $c(n)$, ...] , the predictor computes their output according to

$$\hat{c}(n+N|n)=\sum_{k=0}^{M-1}\omega_k c(n-k), n=1,2,3,\ldots \tag{1}$$

where M is the order of the predictor, N is the number of foreword predictive frames, $\hat{c}(n+N|n)$ is the predicted value. Find recursively

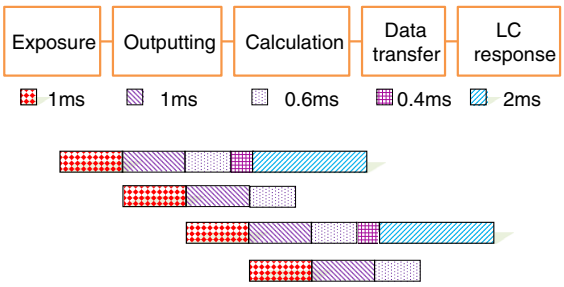

Fig. 2. The time sequence of the liquid-crystal open-loop adaptive optics system.

in time the parameters $\{\omega_1(n), \omega_2(n),\ldots, \omega_M(n)\}$such as to minimize the sum of squared error

$$J(n)=\sum_{i=1}^{n}\lambda^{n-i}\left[e(i)^2\right]=\sum_{i=1}^{n}\lambda^{n-i}\left[c(i+N)-\sum_{k=0}^{M-1}\omega_k c(i-k)\right]^2, \tag{2}$$

where the predictive error signal is

$$e(i)=c(i+N)-\hat{c}(i+N|i)=c(i+N)-\sum_{k=0}^{M-1}\omega_k c(i-k) \tag{3}$$

and the forgetting factorλ reduces the influence of the old data, $0<\lambda\leq 1$. Eq. (2) is a standard least square criterion. If we find a recursive in time way to compute the weight vector $\underline{\omega}(n)$(in this paper, a column vector is marked with an underline), then it yields

$$\underline{\omega}(n)=\underline{\omega}(n-1)+\underline{k}(n)e(n). \tag{4}$$

The apriori error $e(n)$is

$$e(n)=c(n+N)-\underline{c}(n)^T\underline{\omega}(n-1). \tag{5}$$

The RLS gain $\underline{k}(n)$is

$$\underline{k}(n)=\frac{\lambda^{-1}P(n-1)\underline{c}(n)}{1+\lambda^{-1}\underline{c}(n)^T P(n-1)\underline{c}(n),} \tag{6}$$

where $P(n)$is a matrix defined as

$$P(n)=\left[\sum_{i=M+N}^{n}\lambda^{n-i}\underline{c}(i)\underline{c}(i)^T\right]^{-1}. \tag{7}$$

It can also be calculated in a recursive method, which is

$$P(n)=\lambda^{-1}P(n-1)-\lambda^{-1}\underline{k}(n)\underline{c}(n)^T P(n-1). \tag{8}$$

Now we can summarize the RLS modal predictor algorithm as follows [see Fig. 3]. First, when a new Zernike coefficient $c(n+N)$is

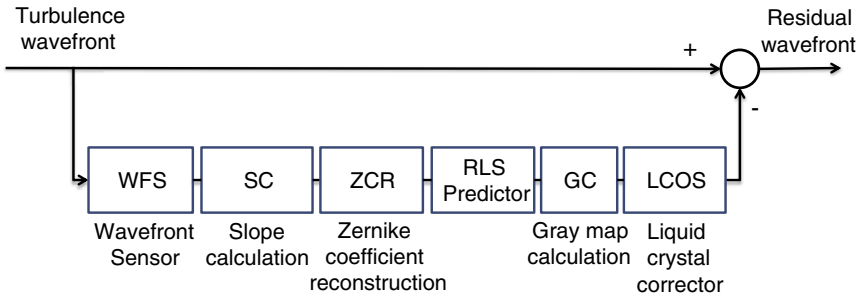

Fig. 1. The diagram of an open-loop liquid-crystal adaptive optics sysem with RLS predictor.

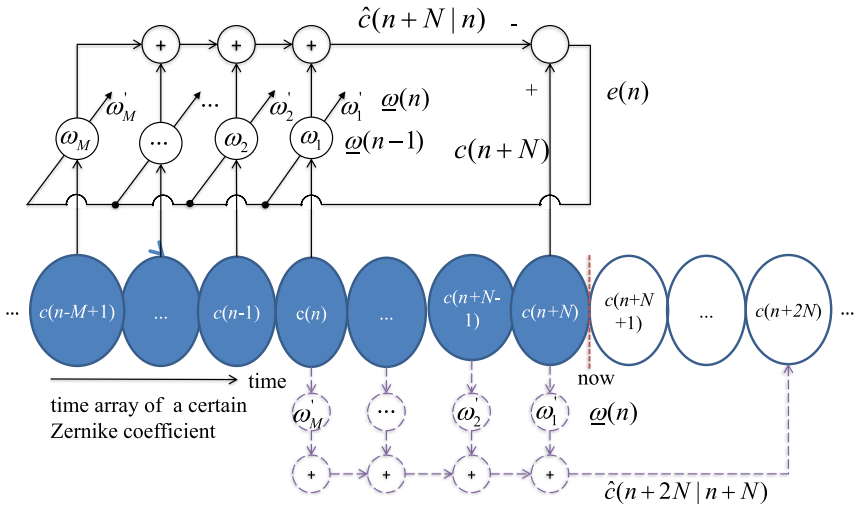

Fig. 3. The schematic diagram of the RLS predictor.

acquired by the RLS predictors, it is used as the desired response of the predictor. Second, use the last vector $\omega(n-1)$ as the weight vector and use the M terms of Zernike coefficients $c(n)$ that N frames back as the input vector to predict the current coefficient$c(n+N)$ with Eq. (1). Third, the apriori error can be calculated by Eq. (5) , and the RLS gain $k(n)$ can be calculated by Eq. (6). Therefore, the weight vector $\omega(n-1)$ can be updated and a new weight vector $\omega(n)$is achieved through the Eq. (4). Fourth, the Zernike coefficient of the Nth frames foreword in the future can be predicted with

$$\hat{c}(n+2N|n+N)=\sum_{k=0}^{M-1}\omega_k(n)c(n+N-k). \tag{9}$$

Last, in order to prepare the calculation for the next loop, the value of $P(n)$has to be calculated with Eq. (8). Up to now, the whole predictive process of a certain Zernike modal coefficient of a single time step is finished. Similarly, the method can be used for the prediction of the other Zernike modal coefficients. After the prediction of the whole modal coefficients that are used in the LC AOS is finished, the RLS predictor waits the next new modal coefficient vector. When a new modal coefficient vector arrives, the predictor increases the time step to $n+1$, and the corresponding predictive steps are the same as the steps introduced above.

There are two variables that need initial values in order to start the recursions. One is the weight vector $\underline{\omega}(0)$and the other is$P(0)$. Typically, the initialization for $\underline{\omega}(0)$is$\underline{\omega}(0)=0$, and for $P(0)$is$P(0)=\delta^{-1}I$, where I is an identity matrix and δ is a relatively small number with a recommended value, $\delta\le 0.01\sigma_c^2$($\sigma_c^2$is the variance of the time array of the Zernike coefficient).

3. Data generation

In order to demonstrate what we can gain by using the RLS predictor instead of a general open-loop modal correction based on the previous detected frame [7], it needs to generate an array of dynamic turbulence wavefront. There are several steps to produce it. First, a big static wavefront with an aperture of D which satisfies Kolmogoroff turbulence spatial statistics has to be obtained. In our simulation, the aperture D equals 4 m and the method of Zernike polynomials is used to simulate the static turbulence wavefront [21]. The Wiener power spectrum of phase fluctuation is used to represent the spatial statistics of Kolmogoroff atmospheric wavefront. The number of the Zernike polynomials used to calculate the wavefront is 496, which makes the structure function of the simulated wavefront satisfy the 5/3 law with negligible error. The aperture D equals to 4000 pixels. Second, the wavefront in a sub-area of the big simulated wavefront is used to simulate the wavefront received in the entrance pupil of a telescope with an aperture of 1.2 m. The Tyler's hypothesis is used to produce the temporal evolution wavefront array. In order to simulate a large number of frames, a random route is used to generate different frames of wavefront. The step length between adjacent frames is $V_{wind}\cdot\Delta t$, where V_{wind} is the wind speed and $\Delta t$is the time interval. The Δtmust be small enough to make the wavefront change fluently. At last, the simulated wavefront in the sub-area is fitted to the first 35 terms of Zernike polynomials coefficients which are sent to the RLS predictor (the actual LC AOS corrects the first 35 terms of Zernike modes excluding piston).

Before generating the dynamic turbulence wavefront data, we set a limit to the turbulence wavefront time array. In adaptive optics systems that do not employ predictive techniques, wind-speed conditions are limited by the correlation between a turbulent wavefront at the time of measurement and the same wavefront at the time of correction. This correlation implies that an adaptive optical system is expected to improve imaging performance when

$$\frac{E[\phi(t)\phi(t+T)]}{E[\phi^2(t)]}\ge\frac{1}{2}, \tag{10}$$

where $\phi(t)$ represents the wavefront at the time of measurement, and$\phi(t+T)$ represents the wavefront at the time of correction. The left-hand side is determined by the system delay T, by the measurement noise ratio N_R, by the Fried Parameter r_0 and by the magnitude of the wind speed V_{wind}. In this paper, each time array of turbulence wavefront we generated is in accordance with Eq. (10).

The measurement noise is also taken into account. In the simulation, the white noise is added into the Zernike coefficients according to the noise ratio (N_R). N_R is expressed as the ratio of the measurement noise standard deviation to the average of the Zernike coefficient standard deviation.

Fig. 4 shows the summation of the power spectrum density (PSD) of the 35 Zernike coefficient time arrays that are produced by the method mentioned above. It illustrates that the PSD is proportion to $f^{-17/3}$at high frequency, which is in accordance with Kolmogorov turbulence [22,23].

4. Prediction test

We first investigated the convergence of the RLS algorithms. Then, in order to choose an appropriate number of the foreword predictive

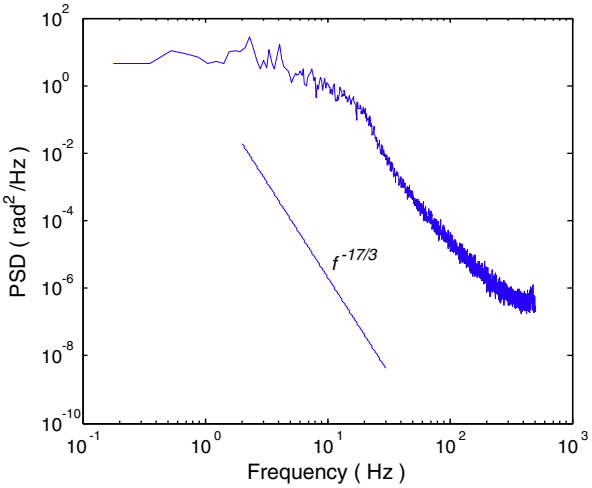

Fig. 4. The summation of the power spectrum density of the first 35 Zernike coefficient time array (piston is excluded). Conditions: $V_{wind}=10$ m/s, $r_0=6$ cm, $f_s=1000$ Hz, $N_R=0\%$, Sample *No.* = 5659.

frame N and the number of predictor order M, we investigated the root mean square (RMS) error with prediction (RMS_{pre}) versus different N and versus different M under several important conditions, such as V_{wind}, Fried parameter r_0, M(only for the choice of N), SLDF, f_s and N_R. Last, we evaluated the predictive performance.

4.1. Convergence of the RLS algorithm

The inputs of the algorithm are the 35 Zernike modal coefficients with white measurement noise added. The algorithm converges quickly in most cases, i.e., in less than 2000 iterations. Fig. 5 shows the convergence of the predictor parameter for the 16th Zernike mode. It can be seen that all these predictor parameters converge after 1500 frames.

4.2. The choice of the number of the foreword predictive frame N

It needs to emphasize that the RMS_{pre} is the *RMS* of the residual wavefront between the predicted wavefront and the true wavefront at the time of correction. The relation between RMS_{pre} and N was calculated with a single variable V_{wind} as shown in Fig. 6(a). The other parameters are all fixed. It is obvious that when N equals to five that is the same as the SLDF, the RMS_{pre} of each curve that with a different fixed V_{wind} reaches its corresponding minimum value. It is demonstrated that when the RLS predictor reaches the minimum predictive error, the choice of N is independent of V_{wind}. Furthermore, when N is smaller or larger than 5, the RMS_{pre} would increase with a speed proportional to V_{wind}. The bigger the V_{wind}, the larger the minimum RMS_{pre} is.

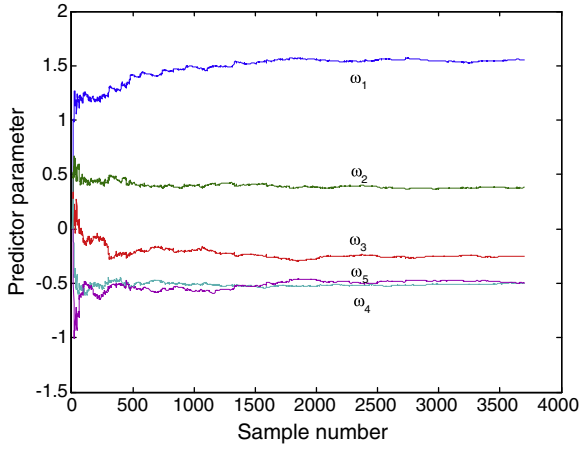

Fig. 5. The convergence of the predictor parameter for the 16th Zernike mode. Conditions: SLDF = 5, $N=5$, $V_{wind}=15$ m/s, $r_0=6$ cm, $f_s=1000$ Hz, $N_R=5\%$.

The relationship between RMS_{pre} and N was also calculated with a single variable r_0 [see Fig. 6(b)], with a single variable M [see Fig. 6(c)] and with a single variable N_R [see Fig. 6(d)]. In all these cases, it is when N equals to SLDF that the RMS_{pre} can reach a minimum value. It shows a fact that the choice of N is independent of r_0, M and N_R when the RLS predictor reaches the minimum predictive error.

In order to confirm the idea that the best N is always equal to SLDF, we calculated the relation between RMS_{pre} and N with a single variable SLDF as shown in Fig. 6(e). It is demonstrated that only when N equals to SLDF, can the RMS_{pre} reach its minimum value. Furthermore, Fig. 6(e) also shows that the minimum RMS_{pre} is proportional to SLDF. When the sampling frequency f_s changes, the SLDF would change accordingly of which the AOS has a constant loop delay time. The RMS_{pre} reaches a minimum value when N equals to the corresponding SLDF as shown in Fig. 6(f). Though more numerical simulation, it confirms us that the best N is only determined by the SLDF.

In order to explain why the best N is only determined by the SLDF, we have researched the RMS error of the residual wavefront between the predicted wavefront and the true wavefront to be predicted versus different predicted time interval. Both of the direct correction method that corrects wavefront based on the previous frame and the RLS predictive method are considered. For the direct correction method, the main residual error is induced by the time delay. However, for the RLS predictive method, the main residual error is determined by the precision of the prediction. As shown in Fig. 7, the predicted error is always smaller than the wavefront error induced by time delay for different time interval. It is also true under different turbulence conditions which are in accordance with Eq. (10). That is the reason why the predictive time must always be equal to the system loop delay time as discussed above. What's more, the longer the predictive time, the bigger the predictive error is. It implies that it is more difficult to predict the wavefront with long time interval.

4.3. The choice of the number of the predictor order M

We calculated the relationship between RMS_{pre} and M with a single variable V_{wind} , r_0, SLDF, f_s and N_R as shown in Fig. 8. As shown in Fig. 8(a)–(d), the RMS_{pre} reaches the minimum value when M is equal or larger than two when N_R equals zero. This phenomenon does not change with the V_{wind} , r_0, SLDF and f_s. However, it is not the same as N_R. When RMS_{pre} reaches the minimum value, for different N_R, it needs a different M as shown in Fig. 8(e). With data under more conditions, we have concluded that the M is only related to the N_R when RMS_{pre} reaches its minimum value.

4.4. Evaluation of the predictive performance

An ordinary open-loop LC AOS corrects the turbulent wavefront based on previous detected frame. However, for an open-loop LC AOS with RLS predictor, it corrects the turbulent wavefront based on the predictive frame. Therefore, we evaluated the RLS predictor performance through comparing it with an ordinary open-loop LC AOS. To quantify what is gained by using the predictor rather than the ordinary LC AOS, we define the following parameters:

$$RMS=\left\langle \sum_{mode}\varepsilon_{mode}^2 \right\rangle^{1/2},\ \eta=1-\frac{RMS_{pre}}{RMS_{unpre}},$$
$$\eta_{mode}=1-\frac{\left\langle \varepsilon_{\mathrm{mode}}^2 \right\rangle_{pre}^{1/2}}{\left\langle \varepsilon_{\mathrm{mode}}^2 \right\rangle_{unpre}^{1/2}},\ S_R=e^{-RMS^2}, \tag{11}$$

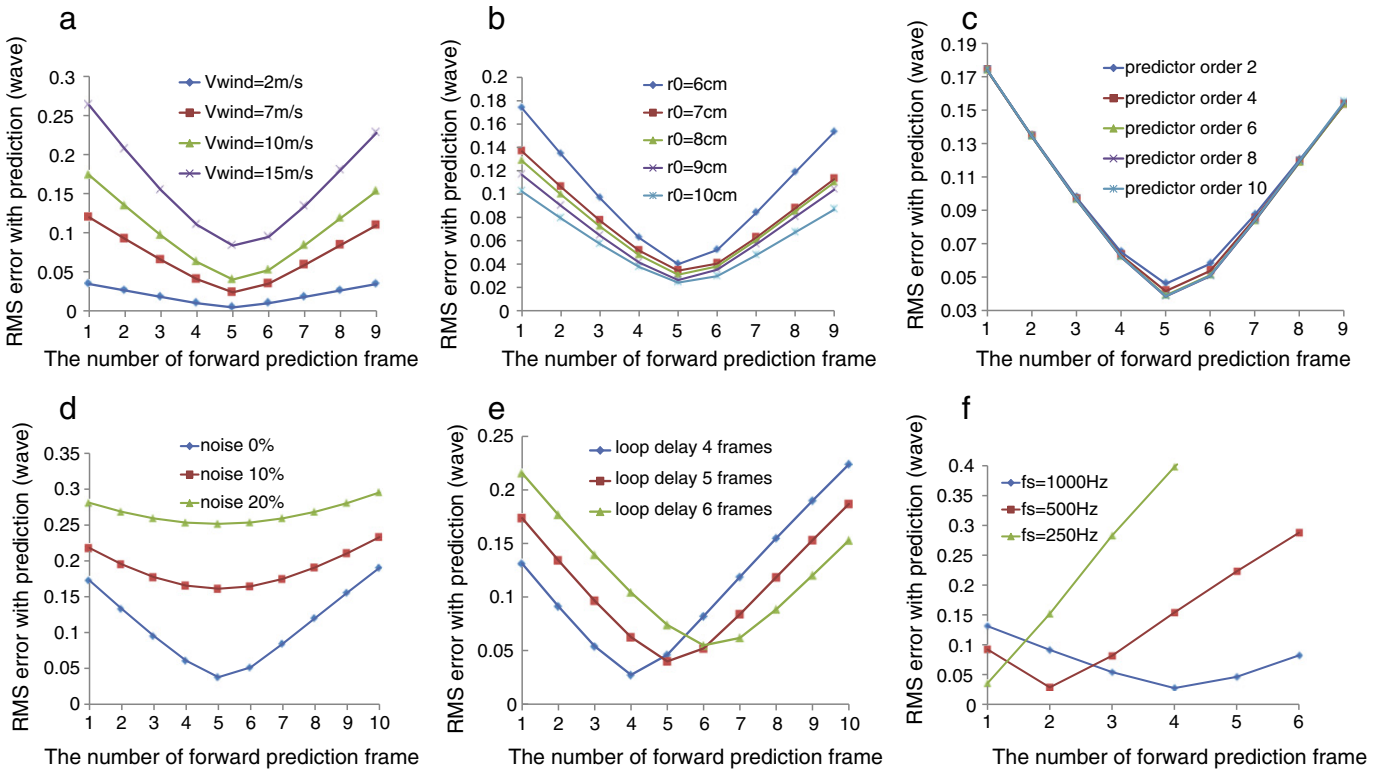

Fig. 6. The RMS predictive error versus different numbers of forward predictive frame under different conditions. (a) SLDF = 5,$M=5$, $r_0=6$ cm, $f_s=1000$ Hz, $N_R=0$; (b) SLDF = 5, $M=5$, $V_{wind}=10$ m/s, $f_s=1000$ Hz, $N_R=0$; (c) SLDF = 5, $V_{wind}=10$ m/s, $r_0=6$ cm, $f_s=1000$ Hz, $N_R=0$; (d) SLDF = 5, $M=5$, $V_{wind}=10$ m/s, $r_0=6$ cm, $f_s=1000$ Hz; (e) $M=5$, $V_{wind}=10$ m/s, $r_0=6$ cm, $f_s=1000$ Hz ,$N_R=0$; (f) SLDF = 1 ($f_s=250$ Hz), SLDF = 2 ($f_s=500$ Hz), SLDF = 4 ($f_s=1000$ Hz), $M=5$, $V_{wind}=10$ m/s, $r_0=6$ cm, $N_R=0$.

where $\varepsilon_{mode}$is the residual Zernike coefficient of mode number *mode*, *RMS* is the root mean square of the total residual wavefront error, RMS_{pre} and RMS_{unpre} are the *RMS* obtained with RLS predictor and an ordinary LC AOS, respectively. $\langle\varepsilon^2_{\mathrm{mod}\ e}\rangle^{1/2}_{pre}$and $\langle\varepsilon^2_{\mathrm{mod}\ e}\rangle^{1/2}_{unpre}$are the root mean square of the Zernike coefficient of mode number *mode* obtained with a RLS predictor and an ordinary LC AOS, respectively. The higher the η or η_{mode}, the more we gain by using the RLS predictor.

We now evaluate the general trend for η or η_{mode} and Strehl ratio S_R. Fig. 9 shows the η versus noise ratio N_R for two f_s. Fig. 10 presents S_R versus N_R for prediction on and off under two different Greenwood frequencies (Fg). When prediction is off, the system equals to an ordinary LC AOS that corrected the wavefront based on the previous measured frames. These two graphs show that the RLS predictor always works better than the corresponding ordinary LC AOS. Fig. 9 demonstrates that the gain η is higher when the N_R is low and f_s is high. This can be interpreted in the following way. When the N_R is high, the measurements is much noisy, which are used as the "truth" of the predictor, causing it to predict wrong wavefront. When f_s is high, the measurement time step is short, which can provide more new messages about the move trend of the turbulent wavefront. As shown in Fig. 10, the S_R is decrease with the N_R and Fg for both RLS predictor and the ordinary LC AOS. When the noise ratio $N_R=0$, the S_R after prediction can reach as high as 90%.

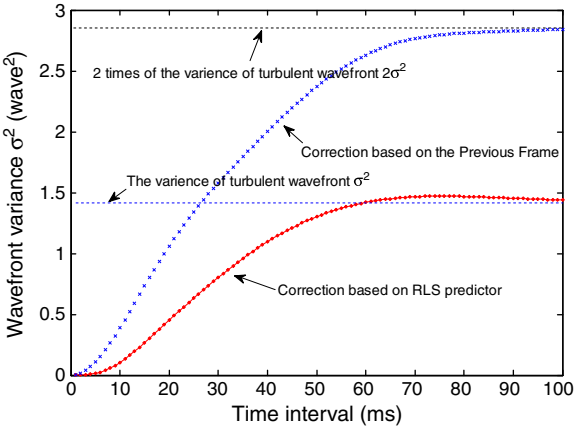

Fig. 7. Wavefront variance versus time interval with and without prediction. Conditions: $M=2$, $V_{wind}=15$ m/s, $r_0=6$ cm, $f_s=1000$ Hz ,$N_R=0$.

Fig. 11 shows the relationship between η_{mode} and Zernike mode index. As the Zernike mode index increasing, η_{mode} is decreasing linearly from 55% to 30%. There are two main reasons for this. First, with the increase of the Zernike mode index, the signal-to-noise ratio of Zernike polynomials which is defined as the ratio of the mode turbulence variance to the variance of the noise propagated on the mode is decreasing. Second, the Zernike mode cutoff frequency increases with the radial order of the Zernike polynomials.

We also compared the predictor with the one worked in a closed-loop system in reference [13]. Both predictors are based on the RLS method. As shown in Fig. 9 of reference [13], the predictive gain of the predictor in closed-loop system is between 45% and 30% for the first 35 Zernike modes. The corresponding Fg is 8.6 Hz ($D/r_0=10$, $V/D=2$ Hz, Fg = 0.43 $V/r_0=8.6$ Hz) and the $N_R=2\%$ (SNR = 50). But for the predictor described in this paper, the predictive gain is between 55% and 30%, which is nearly the same as that of the predictor worked in closed-loop system. However, the corresponding turbulence condition and noise are much more serious. The Fg is 108 Hz ($V_{wind}=15$ m/s, $r_0=6$ cm, Fg = 0.43 $V/r_0=108$ Hz) and the N_R is 5%. So it is obvious that the predictor that works in an open-loop system has much better performances. It is mainly due to the feedback of the closed-loop system. The predictive error in a closed-loop system would be feedback to the system again, which would be added to the import Zernike coefficients of the predictor in next loop. However, the predictor in open-loop system has no such a kind of problem.

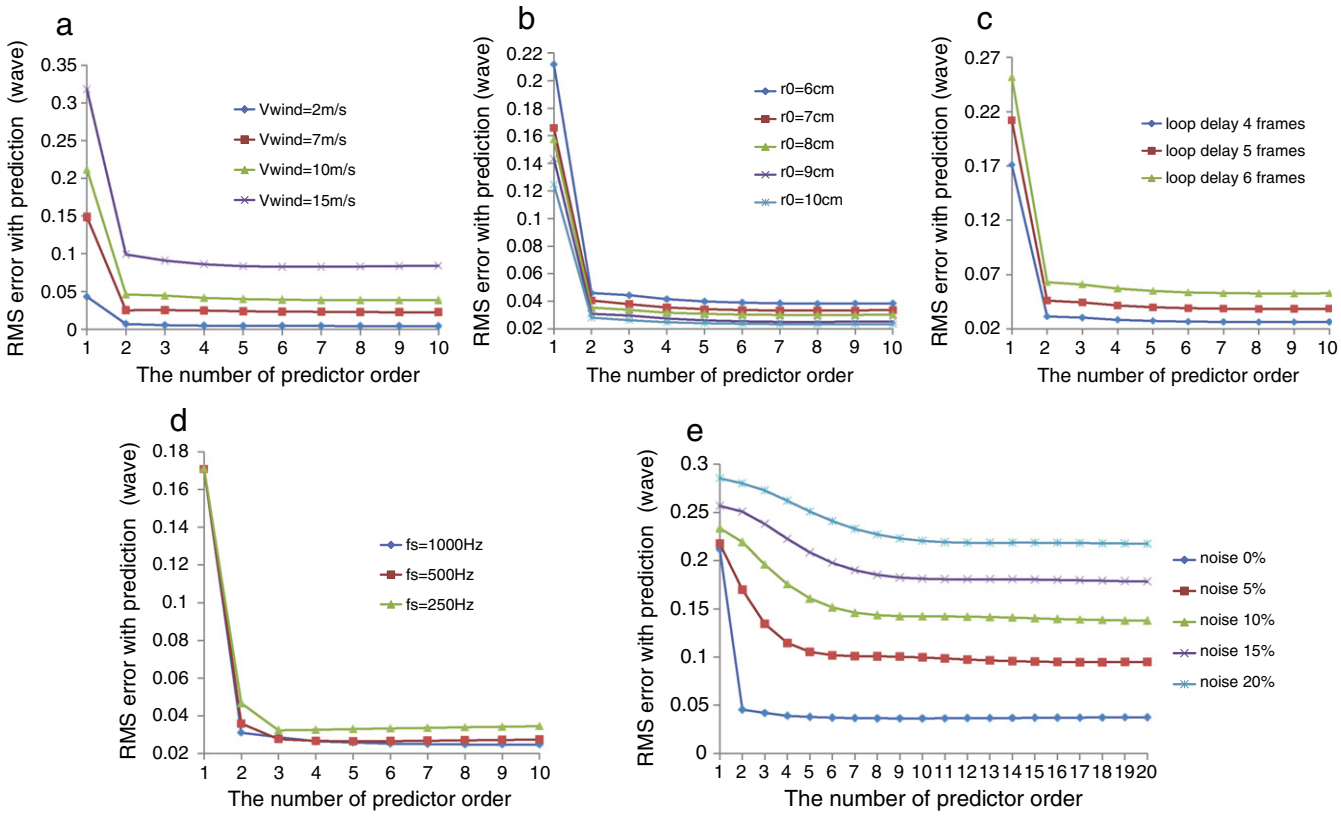

Fig. 8. The RMS predictive error versus different number of predictor order under different conditions. Conditions: (a) SLDF = 5, $N = 5$, $r_0 = 6$ cm, $f_s = 1000$ Hz, $N_R = 0$;(b) SLDF = 5, $N = 5$, $V_{wind} = 10$ m/s, $f_s = 1000$ Hz, $N_R = 0$;(c) N = SLDF, $V_{wind} = 10$ m/s, $r_0 = 6$ cm, $f_s = 1000$ Hz, $N_R = 0$; (d) SLDF = 1(fs = 250 Hz), SLDF = 2(fs = 500 Hz), SLDF = 4(fs = 1000 Hz), N = SLDF, $V_{wind} = 10$ m/s, $r_0 = 6$ cm, $N_R = 0$; (e) SLDF = 5, $N = 5$, $V_{wind} = 10$ m/s, $r_0 = 6$ cm, $f_s = 1000$ Hz.

5. Conclusion

In this paper we investigated the modal RLS prediction that used on the open-loop liquid-crystal adaptive optics systems, which has a simple architecture, low computational complexity and a high converging speed. The impact of the number of the foreword predictive frame N and the number of predictor order M of the RLS predictor is analyzed respectively. The results demonstrated that the best foreword predictive frame N must equal to the system loop delay frame SLDF since the predictive error is always smaller than the corresponding time delay error. The appropriate predictor order M of the RLS predictor is equal to 2 or 3 when there is no measurement noise and it depends on noise ratio N_R when the measurement error cannot be neglected. For an ordinary turbulent condition with Greenwood frequency of 63 Hz, the open-loop LC AOS with RLS prediction can reach a gain as high as about 70% than the same open-loop LC AOS without prediction and the S_R can reach about 0.7 from 0.02 when there is no measurement error. With the increase of the noise ratio N_R, the predictive gain and the Strehl ratio is decreasing. With the increase of the sampling frequency, the predictive gain is increasing. However, when the turbulence becomes more fast, the predictive gain would decrease. In the near further, we will publish the results obtained from a real open-loop LC AOS system under real turbulent condition.

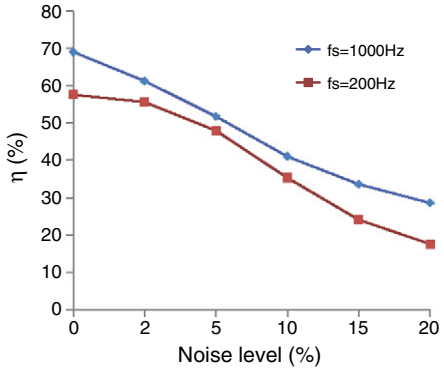

Fig. 9. Predictive gain versus noise level. Conditions: SLDF = 5, $N = 1(f_s = 200$ Hz), $N = 5(f_s = 1000$ Hz), $V_{wind} = 15$ m/s, $r_0 = 6$ cm, $M = 2(N_R = 0\%)$, $M = 3(N_R = 2\%)$, $M = 5(N_R = 5\%)$, $M = 7(N_R = 10\%)$, $M = 8(N_R = 15\%)$, $M = 9(N_R = 20\%)$.

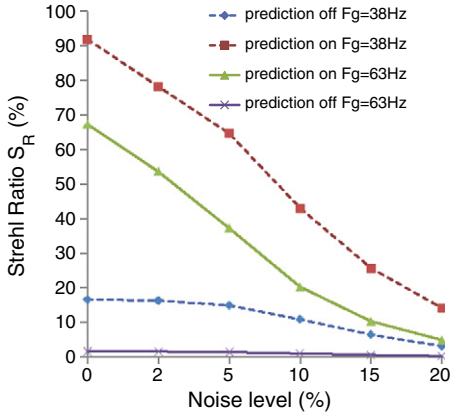

Fig. 10. Strehl ratio versus nosie leveal with and without prediction. Conditions: SLDF = 5, $N = 5$, $f_s = 1000$ Hz, $M = 2(N_R = 0)$, $M = 3(N_R = 2\%)$, $M = 5(N_R = 5\%)$, $M = 7$ $(N_R = 10\%)$, $M = 8(N_R = 15\%)$, $M = 9(N_R = 20\%)$.

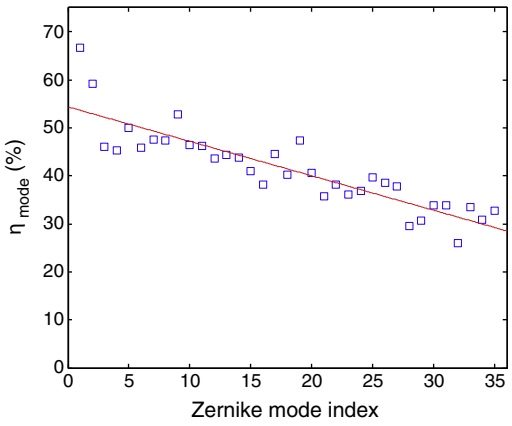

Fig. 11. The predictive gain of different zernike modes. Conditions: SLDF = 5, $N = 5$, $V_{wind} = 15$ m/s, $r_0 = 6$ cm, $f_s = 1000$ Hz, $N_R = 5\%$.

Acknowledgment

This work is supported by the National Natural Science Foundation (No. 60736042, No. 60578035, and No. 50703039). The authors also gratefully acknowledge all the referees' efforts and suggestions.

References

[1] G. Love, Applied Optics 36 (1997) 1517.
[2] P. Prieto, E. Fernandez, S. Manzanera, P. Artal, Optics Express 12 (2004) 4059.
[3] J. Schmidt, M. Goda, B. Duncan, Applied Optics 46 (2007) 2423.
[4] C. Li, M. Xia, Q. Mu, B. Jiang, L. Xuan, Z. Cao, Optics Express 17 (2009) 10774.
[5] Q. Mu, Z. Cao, D. Li, L. Hu, L. Xuan, Applied Optics 47 (2008) 4297.
[6] C. Li, M. Xia, D. Li, Q. Mu, L. Xuan, Journal of Biomedical Optics 15 (2010) 046009.
[7] C. Liu, L. Hu, Q. Mu, Z. Cao, L. Xuan, Applied Optics 50 (2011) 82.
[8] C. Schwartz, G. Baum, E.N. Ribak, Journal of the Optical Society of America. A 11 (1994) 444.
[9] G.J. Aitken, D. McGaughey, in: Proceedings of Topical Meeting on Adaptive Optics, M. Cullum (Eds.), European Southern Observatory, Garching, Germany, European Southern Observatory, Garching, Germany, 1995, p. 89.
[10] R. Paschall, D. Anderson, Applied Optics 32 (1993) 6347.
[11] W. Wild, Optics Letters 21 (1996) 1433.
[12] C. Dessenne, P.Y. Madec, G. Rousset, Optics Letters 22 (1997) 1535.
[13] C. Dessenne, P.-Y. Madec, G. Rousset, Applied Optics 37 (1998) 4623.
[14] C. Dessenne, P.Y. Madec, G. Rousset, Optics Letters 24 (1999) 339.
[15] L. Poyneer, J. Véran, Journal of the Optical Society of America. A 25 (2008) 1486.
[16] M. Lloyd-Hart, P. McGuire, in: M. Cullum (Ed.), Proceedings of Topical Meeting on Adaptive Optics, European Southern Observatory, Garching, Germany, 1995, p. 95.
[17] P. McGuire, T. Rhoadarmer, H. Coy, J. Angel, M. Lloyd-Hart, Proceedings of SPIE 4007 (2000) 682.
[18] M. Jorgenson, G. Aitken, Optics Letters 17 (1992) 466.
[19] M.B. Jorgenson, G.J.M. Aitken, Proceedings of SPIE 1706 (1992) 113.
[20] D. Montera, B. Welsh, M. Roggemann, D. Ruck, Applied Optics 36 (1997) 675.
[21] N. Roddier, Optical Engineering 29 (1990) 1174.
[22] H. Jakobsson, Applied Optics 35 (1996).
[23] J.-M. Conan, G. Rousset, P.-Y. Madec, Journal of the Optical Society of America. A 12 (1995) 1559.